EXPERIMENTAL STUDIES OF THE COLLISIONAL EXCITATION OF INFRARED ACTIVE VIBRATIONAL STRETCH MODES IN CO_2 AND H_2O WITH AN INTERSECTING, HYPERTHERMAL MOLECULAR BEAM APPARATUS. VOLUME 1

C. E. Kolb, et al

Aerodyne Research, Incorporated

Prepared for:

Air Force Rocket Propulsion Laboratory
Yale University

February 1975

UNCLASSIFIED

SECURITY CLASSIFICATION OF THIS PAGE (When Data Entered)

REPORT DOCUMENTATION PAGE		READ INSTRUCTIONS BEFORE COMPLETING FORM
1. REPORT NUMBER AFRPL-TR-75-2	2. GOVT ACCESSION NO.	3. RECIPIENT'S CATALOG NUMBER AD/A-006237
4. TITLE (and Subtitle) Experimental Studies of the Collisional Excitation of Infrared Active Vibrational Stretch Modes in CO_2 and H_2O With an Intersecting Hyperthermal Molecular Beam Apparatus		5. TYPE OF REPORT & PERIOD COVERED Final Report 6. PERFORMING ORG. REPORT NUMBER ARI-RR-55
7. AUTHOR(s) C.E. Kolb/M. Camac Aerodyne Research, Inc., R.B. Subbarao/J.B. Anderson Yale University		8. CONTRACT OR GRANT NUMBER(s) F04611-73-C-0050
9. PERFORMING ORGANIZATION NAME AND ADDRESS Aerodyne Research, Inc., 20 South Avenue Burlington, Massachusetts 01803		10. PROGRAM ELEMENT, PROJECT, TASK AREA & WORK UNIT NUMBERS 5730 BPSN 625730
11. CONTROLLING OFFICE NAME AND ADDRESS Air Force Rocket Propulsion Laboratory/AFSC Edwards, CA 93523		12. REPORT DATE February 1975 13. NUMBER OF PAGES 48
14 MONITORING AGENCY NAME & ADDRESS(if different from Controlling Office) --		15. SECURITY CLASS. (of this report) Unclassified 15a. DECLASSIFICATION/DOWNGRADING SCHEDULE N/A

16. DISTRIBUTION STATEMENT (of this Report)

APPROVED FOR PUBLIC RELEASE: DISTRIBUTION UNLIMITED

17 DISTRIBUTION STATEMENT (of the abstract entered in Block 20, if different from Report)

18 SUPPLEMENTARY NOTES

19. KEY WORDS (Continue on reverse side if necessary and identify by block number)

rocket plume radiation
infrared radiation
molecular beams
energy transfer

20 ABSTRACT (Continue on reverse side if necessary and identify by block number)

An intersecting, hyperthermal energy molecular beam apparatus with a liquid nitrogen colled infrared radiation detector system designed to measure T-V coll sional excitation cross sections for the infrared active modes of small molecules is d ribed in this report. In addition, a novel infrared calibration technique using the elf-emission of a molecular beam containing H_2O or CO_2 formed by supersonic expansion from a high temperature nozzle is presented and the design and testing of

DD FORM 1 JAN 73 1473 EC

UNCLASSIFIED
SECURITY CLASSIFICATION OF THIS PAGE (When Data Entered)

ABSTRACT (Cont.)

a dc arc heated supersonic nozzle source for producing molecular beams of atomic oxygen seeded in noble gases is discussed.

Measured upper bounds for T-V excitation of the CO_2 and H_2O ν_3 vibrational modes in collision with N_2 at several relative collision velocities in the range of 4 to 8 km/second are presented and compared to literature values for total scattering cross sections of CO_2 and H_2O as well as to previous experimental and theoretical determinations of CO_2 and H_2O ν_3 activation cross sections.

NOTICES

When U.S. Government drawings, specifications, or other data are used for any purpose other than a definitely related Government procurement operation, the Government thereby incurs no responsibility nor any obligation whatsoever, and the fact that the Government may have formulated, furnished, or in any way supplied the said drawings, specifications, or other data, is not to be regarded by implication or otherwise, or in any manner licensing the holder or any other person or corporation, or conveying any rights or permission to manufacture, use or sell any patented invention that may in any way be related thereto.

FOREWORD

This report was submitted by Aerodyne Research, Incorporated, 20 South Avenue, Burlington, MA 01803, under Contract F04611-73-C-0050, Job Order No. 573009BU with the Air Force Rocket Propulsion Laboratory, Edwards, CA 93523.

This report has been reviewed by the Information Office/DOZ and is releasable to the National Technical Information Service (NTIS). At NTIS it will be available to the general public, including foreign nations.

Larry P. Davis

LARRY P. DAVIS, 1Lt. USAF
Project Scientist

J. Daniel Stewart

J. DANIEL STEWART, GS-14
Manager, Plume Technology

FOR THE COMMANDER

Paul J. Daily

PAUL J. DAILY, Colonel, USAF
Chief, Technology Division

TABLE OF CONTENTS

LIST OF ILLUSTRATIONS

LIST OF TABLES

1. INTRODUCTION

The experiment described in this report was designed to study the collisional activation of infrared active vibrational stretch modes in combustion exhaust gases such as water and carbon dioxide. Molecular beams of exhaust species, as well as beams of collision partners such as N_2 and O_2, were prepared by seeding the desired beam species in helium or hydrogen gas and expanding the mixture through heated supersonic nozzles into a collision chamber. The intersection of two such beams permitted the study of exhaust gas-collision partner interactions over a relative velocity range of 4 to 8 km/sec which corresponds to a center of mass collisional energy range of 1 to 6 eV. The partial development of a dc arc heated atomic oxygen seeded nozzle beam source is also described.

The interaction region of the colliding molecular beams was placed at the focal point of a liquid nitrogen cooled optical train which included an InSb photovoltaic infrared detector. This detector was designed to monitor the infrared light emitted by vibrationally excited exhaust species. Knowledge of the level of infrared radiation caused by the interaction of the colliding beams was then combined with experimental parameters such as beam density and velocity, and molecular parameters such as radiative lifetimes to determine upper limits for the collisional activation cross sections for the infrared active stretch modes of H_2O and CO_2 with various collision partners.

Molecular parameters of the pertinent H_2O and CO_2 vibrationally excited states are reviewed in the following section along with previous experimental and theoretical studies concerning the collisional activation of these states. Section 3 contains a description of the experimental apparatus, as well as the results of various calibration measurements. Section 4 describes the data analysis methods used in this study, while Section 5 presents the experimental results obtained. Section 6 contains a discussion of the results obtained along with recommendations for future studies.

2. REVIEW OF MOLECULAR DATA AND PREVIOUS STUDIES

2.1 Vibrational Band Parameters

Water and carbon dioxide are major equilibrium exhaust products resulting from the near stoichiometric combustion of hydrocarbons with nonhalogen oxidizers in rocket motor combustion chambers. Both the ν_1 and ν_3 stretch modes of H_2O are infrared active and form a single infrared band near 2.7μ. Since CO_2 is linear molecular its ν_1 symmetric stretch mode does not radiate, however, its asymmetric stretch fundamental mode near 4.3μ is infrared active. The ν_2 bending modes of CO_2 and H_2O at 15 and 6.3μ, respectively, are not of interest in this study since they lie outside the 1.5 to 5.5μ detectibility limits of the InSb detector.

In addition to the fundamental H_2O and CO_2 vibrations noted above, combination and overtone bands are possible contributors to CO_2 and H_2O radiation in the 1.5 to 5.5μ range. However, both combination and overtone bands are usually much weaker radiators than fundamental modes of comparable frequency because of the shorter radiative lifetimes normally found for single quantum transitions. The radiative lifetimes for the H_2O ν_1 and ν_3 fundamentals and the CO_2 ν_3 fundamental along with lifetimes for the strongest overtone and combination bands were needed to design the experiment. The radiative lifetimes for these transitions may be calculated from published integrated band absorption intensities. However, in those cases where one or more transition contributes to a given absorption band, care must be taken to establish band absorption intensities and band radiative lifetimes for each separate vibrational mode.

The inversion of absorption intensities to radiative lifetimes was accomplished using relationships parallel to those developed by Penner[1] between the absorption intensity $S_\nu^{\nu'}$ and the Einstein A coefficient $A_\nu^{\nu'}$:

$$\tau_{rad} = \frac{1}{A_{\nu'}} = \frac{c}{8\pi} \frac{N}{p} \frac{g'}{g} \frac{1 - e^{(-h\nu_o/kT)}}{\nu_o^2 \; S_{\nu'}} \qquad (1)$$

where c is the speed of light, N is the number density of absorbing molecules in the ground state, p is the partial pressure of the absorbing molecules, g and g' are the degeneracies of the lower and upper states of the transition in question, ν_o is the band center frequency, h is Plank's constant, k is Boltzmann's constant and T is the temperature of the absorbing gas. For absorption intensity measurements in the short wavelength infrared at standard temperature and pressure, Eq. (1) reduces to:

$$\tau_{rad}(sec) = \frac{3.210 \times 10^{28}}{S_{\nu'}^{1} (cm^{-2} atm^{-1}) \nu_o^2 (sec^{-2})} \qquad (2)$$

Calculated radiative lifetimes for the transitions of interest are listed in Table I along with band center wavelengths as tabulated by Herzberg.[2] Best values of integrated absorption intensities from the literature are indicated in Table I. Relative contributions of the ν_1, ν_3, $2\nu_2$ modes to the H_2O 2.7μ band used in assessing individual mode absorption intensities are those listed by Gates, et.al.[4]

TABLE I

RADIATIVE LIFETIMES OF INFRARED ACTIVE MODES

Molecule	Transition	λ_o (μ)	Lifetime (msec)	Reference
H_2O	011 → 000	1.88	65	3
	001 → 000	2.66	17	3,4
	100 → 000	2.74	180	3,4
	020 → 000	3.17	2400	3,4
CO_2	$00^0 1 \rightarrow 00^0 0$	4.26	2.4	5
	$10^0 1 \rightarrow 00^0 0$	2.69	60	6
	$02^0 1 \rightarrow 00^0 0$	2.76	79	6

2.2 Previous Experimental Collisional Excitation Studies

Relatively little experimental information is available on the direct collisional excitation of infrared active stretch modes of H_2O and CO_2. The only previous experimental study appears to be the shock tunnel-IR emission study at Calspan, Inc., by Dunn, et.al.[7] This study yielded an upper limit for the activation cross section divided by the band radiative lifetime of H_2O modes radiating in the bandpass from 2.46 to 3.13μ of 3.7×10^{-17} cm^2/sec for N_2 - H_2O collisions at a relative velocity of 5.8 km/sec. The same parameter was determined to be 1.1×10^{-16} for atomic oxygen-H_2O collisions at a relative velocity of 4.3 km/sec. In addition, a partial cross section/radiative lifetime value for CO_2 ν_3 mode activation of 7×10^{-18} was determined by observing the partial 4.3 band emission with a filter passing 4.28 to 4.34μ radiation. Using the H_2O and CO_2 ν_3 radiative lifetimes from Table I allows the following determinations to be made from the Calspan results in Table II:

TABLE II

CALSPAN COLLISIONAL EXCITATION RESULTS

Exhaust Species	Collision Partner	Relative Velocity (km/sec)	ν_3 Excitation Cross Section (cm^2)
H_2O	N_2	5.8	$<6.8 \times 10^{-19}$
H_2O	O	4.3	5.1×10^{-19}
CO_2	N_2	5.8	$\geq 1.7 \times 10^{-20}$

The results for H_2O listed in Table II above, assume that the radiation observed (or not observed) was from the ν_3 fundamental since this state has a far shorter radiative lifetime than either the ν_1 or 2 ν_2. Some doubt exists about the accuracy of the experimental method used in the study of Dunn, et.al. because collisionally activated molecules may have undergone several collisions before entering the detector's field-of-view. This could result in both the partial quenching of vibrationally excited states, and perhaps more significantly, the severe alteration of the expected velocity distribution of excited species passing through the detector's field-of-view.

2.3 Theoretical Collisional Excitation Studies

Theoretical calculations of translation to vibration collisional excitation for the vibrational modes of CO_2 and H_2O with a number of collision partners have been presented in a series of publications by Marriot.[8] These calculations employed a close coupling quantal treatment whose most severe approximations are the complete decoupling of rotational and vibrational modes, and the assumption of a spherically symmetric scattering potential. The collision energies treated in Marriot's calculations generally range from 0.7 to 2.5 eV. The results of Marriot's calculations have been reviewed and fit to an analytical form by Fisher.[9] Fisher also integrated the velocity dependent cross sections into a Maxwell-Boltzmann velocity distribution to yield excitation rate constants and their inverse, collisional quenching rate constants, in order to compare Marriot's calculations with experimental data. In general, collisional quenching rates predicted from Marriot's calculations lie within a factor of 50 of experimentally determined rates.[9] Predictions for collision excitation from the ground state to ν_1, ν_3 and $2\nu_2$ states of H_2O and the ν_3 state of CO_2 for collision energies of 2.5 eV are shown in Table III. It is clear that the magnitude of collisional excitations cross sections predicted by Marriot are considerably larger than cross sections for collisions of comparable energy as measured by the Calspan group.

Most theoretical studies of translation to vibration energy exchange in the literature have been limited to atom-diatomic molecule cases. Marriot's results represent the only direct theoretical study available for collisional activation of the infrared active modes of interest. However, collisional activation cross sections of similar magnitudes at comparable energies for excitation of the CO_2 ν_1 and ν_2 modes by atomic oxygen have been computed by Bass using a classical, hard spheres collision model which retains the anisotropy of the O - CO_2 scattering potential.[10] Similar calculations on the vibrational and rotational excitation of diatomic hydride molecules such as OH, HCl, and HF in atom-molecule collisions at energies above 1 eV by Tait, et.al., also indicated vibrational excitation cross sections of about the same magnitude as those calculated by Marriot for H_2O.[11]

TABLE III

MARRIOT'S THEORETICAL COLLISIONAL EXCITATION CROSS SECTIONS AT 2.5 eV

Exhaust Species	Collision Partner	Excitation Mode	Excitation Cross Section (cm^2)
H_2O	H_2	ν_1	1.6×10^{-17}
		ν_3	3.6×10^{-18}
		$2\nu_2$	9.8×10^{-17}
	H_2O	ν_1	3.5×10^{-18}
		ν_3	6.7×10^{-18}
		$2\nu_2$	1.4×10^{-17}
	CO_2	ν_1	3.2×10^{-19}
		ν_3	1.2×10^{-19}
		$2\nu_2$	1.8×10^{-19}
CO_2	H_2	ν_3	3.8×10^{-17}
	H_2O	ν_3	2.3×10^{-17}
	CO_2	ν_3	5.3×10^{-18}

2.4 Excitation Rate Constants From Collisional Quenching Experiments

Some information about collisional activation cross sections can be gathered from measurements of the reverse process, the quenching of vibrationally excited H_2O or CO_2 by various collision partners. The forward process of vibrational activation and the reverse process of vibrational quenching are related by detailed balancing, as long as the process is direct and does not involve intermediate steps in either direction. Another way of stating this criteria is that the process must be actually reversible, i.e., T -V

activation must be compared to V-T quenching and not V-R quenching. If the process in question meets the above criteria, then the collisional activation rate constant, k_{act}, can be written in terms of the quenching rate constant k_q, in the form:

$$k_{act} = k_q \, e^{-h\nu_o/kT} \tag{3}$$

which reduces to k_{act} equals k_q for k_{act}'s measured at very high temperatures (or collision energies) as in the Calspan experiment.

Unfortunately, it is not clear that available quenching rate constants for the 2.7μ band of H_2O and 4.3μ band of CO_2 can be identified with k_{act} since it is quite possible that these rate constants represent deactivation to either the ν_2 bending modes of CO_2 or H_2O or represent quenching to highly excited rotational modes of the molecule. It should be noted that the colliding species in the experiments described in this report as well as the Calspan experiments are rotationally cold, while molecules in high temperature quenching experiments are usually rotationally hot. In any event, the measured k_q's for CO_2 and H_2O do represent upper limits for k_{act}'s.

Quenching rates are available for a number of processes of interest, for example, Center and Kung have measured k_q for the quenching of H_2O ν_3 by H_2O in the temperature range of 2000-3000°K.[12] They have found that the water-water 2.7μ quenching rate in this temperature range is 4×10^{-11} cm^3/sec. Similar measurements have been performed by Center and Kung on H_2O 2.7μ quenching by Ar,[12] by Center[13] and by Crump and Lambert[14] on 4.3μ quenching of CO_2 by O atoms, and by Heller and Moore[15] on the quenching of the CO_2 4.3μ state by H_2O. These quenching rate constants are tabulated in Table IV.

It is interesting to note that the quenching of CO_2 by O is two orders of magnitude faster than quenching by N_2,[14] which indicates the possible importance of vibrational excitation processes involving atomic oxygen. An impressive number of quenching rates for both the ν_3 and ν_2 states of CO_2 have been previously tabulated by Buchwald and Bauer,[16] and are also available.

TABLE IV

EXAMPLES OF QUENCHING RATE CONSTANTS

Molecule-Mode	Quencher	Temperature Range (°K)	k_q (cm^3/sec)	Reference
H_2O (ν_3)	H_2O	2000-3000	4×10^{-11}	12
	Ar	2000-3000	7×10^{-13}	12
CO_2 (ν_3)	O	300	2×10^{-13}	14
	O	2000-4000	4×10^{-12}	13
	H_2O	300-550	1×10^{-12}	15

Equivalent rate constants for the excitation of H_2O and CO_2 ν_3 modes can be derived by multiplying the collisional velocities and activation cross sections measured by Dunn, et.al., in Table II. Since the collision energies in Dunn's experiments were well above $h\nu_o$ for both the CO_2 and H_2O ν_3 modes these k_{act}'s can be directly compared with the upper limit for k_{act}'s represented by the k_q's in Table IV. The k_{act}'s derived in this manner are $< 3.7 \times 10^{-13}$ and 2.2×10^{-13} for excitation of the ν_3 mode of H_2O by N_2 and O, respectively, and $\geq 9.9 \times 10^{-15}$ for excitation of CO_2 ν_3 by N_2. Thus, the activation rate constants derived from Dunn's data are significantly lower than the upper limits represented by the collisional quenching rates in Table IV.

2.5 Summary of Review Section

As indicated in the foregoing review of available information on the collisional activation of the infrared active stretch modes of CO_2 and H_2O, there is a great deal of conflict in existing experimental and theoretical data. The purpose of the study reported in the following sections was to obtain additional experimental data in the hope of clarifying this situation.

3. EXPERIMENTAL APPARATUS AND TECHNIQUE

The experimental technique utilized to gather information about the collisional excitation of the infrared active vibrational modes of CO_2 and H_2O in this study involve the detection of infrared radiation from collisionally activated CO_2 or H_2O. These activated molecules are prepared under single collision conditions in opposed high velocity flows, one of which contains H_2O or CO_2 while the other contains a molecular collision partner. Hyperthermal velocity flows are required since the threshold activation energy of the H_2O and CO_2 ν_3 modes are 0.466 and 0.291 eV, respectively, both of which require relative collision velocities of greater than 1 km/sec before collision partners of moderate molecular weight can reach the threshold for translation to vibration energy exchange.

The experimental apparatus and techniques utilized to prepare suitable hyperthermal gas flows, as well as the detection system designed to detect the resulting infrared radiation will be described in this section. Subsection 3.1 will outline the construction of the high temperature, seeded nozzles used to produce hyperthermal beams of molecular species. It will also describe the calibration measurements performed for these beams. Subsection 3.2 will present a description of the design, development and testing of a dc arc heated nozzle source for an atomic oxygen beam. Subsection 3.3 will describe the high vacuum collision chamber which contains the experiment. Finally, Subsection 3.4 will describe the design and calibration of the infrared optical detection system and associated electronics.

3.1 Supersonic Nozzle Design and Utilization

Figure 1 shows the schematic arrangement of the nozzles used in the investigation. The nozzles are 1/8 in. o.d., 3 in. long rhenium tubes with a wall thickness of 0.01 in. One end of these tubes was closed by vapor deposition and a hole was cut in the center of the closed end using an electron beam to provide the required nozzle opening. Throat diameter of nozzle 1 is 0.0103 cm and that of nozzle 2 is 0.00785 cm. Nozzles used were supplied by the Rembar Company, Incorporated, New York.

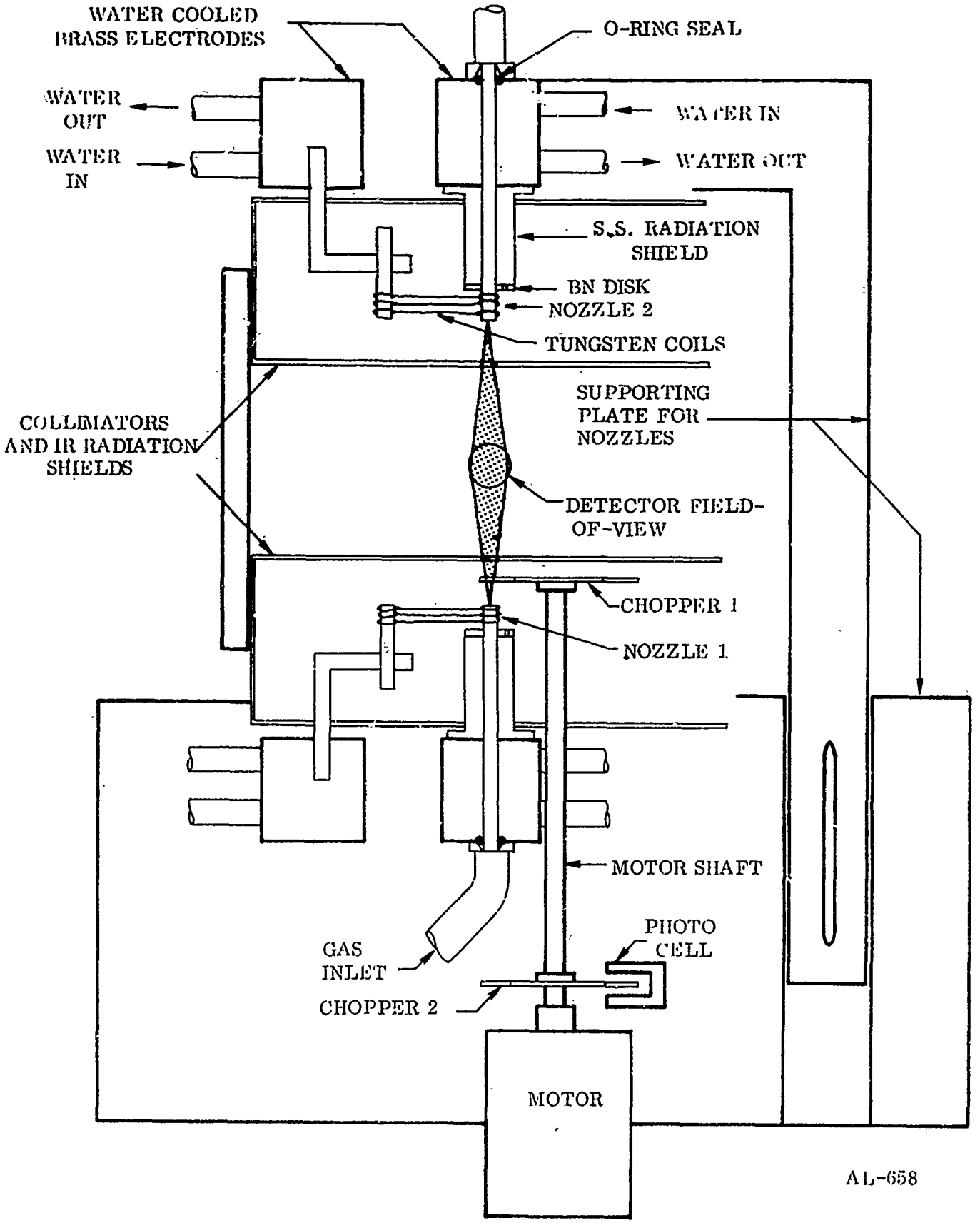

FIGURE 1 SKETCH OF HOT NOZZLE BEAM SOURCES FOR A BEAM INTERACTION ANGLE OF 180°

Each of these tubes was held in a water cooled brass block for heating, and the source gas was introduced through an O-ring sealed junction at the rear. The nozzles were heated by current passed directly through the rhenium tube and out a spring-loaded connection (consisting of tungsten wires 0.015 in. thick) near the tip. A stainless steel radiation shield and boron nitride plug surrounded each of these tubes and kept them aligned. The nozzles were heated to 2100°K with less than 0.010 cm movement of the orifice out of alignment, since the thermal expansion occurs in the axial direction. Water cooled copper radiation shields are used in some experiments to reduce the background radiation. Both high pressure, free-jet sources are mounted on mechanical slide mechanisms for optimum positioning.

Two different methods were employed to measure the source gas temperatures. In the first one, nozzle tip temperatures were obtained from thermocouples mounted directly on the tip of the nozzles. The thermocouples used are 95% tungsten, 5% rhenium and 74% tungsten, 26% rhenium (supplied by Omega Engineering, Incorporated of Stamford, Connecticut). In the second method, a micro-optical pyrometer (from the Pyrometer Instrument Co., Incorporated, Northvale, New Jersey) was used to determine the nozzle tip temperature. The temperatures obtained by these two methods agreed within 20°C. Time-of-flight calibration measurements indicated that the source gas temperature follows the nozzle tip very closely.

Nozzle stagnation pressures were measured with a 60 in. Meriam mercury monometer, Model No. 20 BA 10 WM, and the accuracy of this method is within a few torr.

The research grade gas mixtures shown in Table V were supplied by Matheson Gas Products, Incorporated and were used as source mixtures in this investigation. Care was taken in handling these gases to insure that the gas lines were clean and free from any water vapor.

TABLE V

COMMERCIALLY SUPPLIED NOZZLE SOURCE GASES

Mixture Number	1	2	3	4	5	6
Carrier Gas	H_2 95%	H_2 95%	H_2 90%	H_2 90%	H_e 90%	H_e 90%
Heavier Gas	N_2 5%	CO_2 5%	CO_2 10%	N_2 10%	CO_2 10%	N_2 10%

A 5% H_2O - 95% H_2 gas mixture was obtained by passing 380 torr of H_2 through distilled water in a conical flask at 297°K (the vapor pressure of water at 297°K is about 20 torr). Enough time was allowed for a proper mixing of these two species before feeding the gas into the nozzle.

All the data reported in Section 5 corresponds to the 95% H_2 mixtures since they produced the maximum kinetic energy upon supersonic expansion.

The beam from nozzle 1 is modulated using a two-blade, aluminum chopper (1 3/16 in. in diameter by 1/32 in. thick) to improve the signal-to-noise ratio by converting the dc experiment into an ac experiment. The chopper is driven in a J49 single ϕ, capacitor motor (from Eastern Air Devices Company) at 50 Hz. Because of the two blades, the beam was modulated at a frequency of 100 cycle/sec.

The mean kinetic energy of a single component beam in an expansion can be obtained from energy balance, and is given by:

$$E_i = \frac{1}{2} m v_i^2 = \int_T^{T_o} C_p \, dT \, . \tag{4}$$

For complete expansion $T = 0^o$, and the resulting terminal kinetic energy is given by:

$$\bar{E}_T = \frac{1}{2} \dot{m} V_T^2 = \int_o^T C_p \, dT = \frac{\gamma}{\gamma - 1} R T_o, \tag{5}$$

(for a constant C_p) where T_o is the source temperature, V_T is the terminal velocity, m is the mass of gas species, and, γ is the ratio of its specific heats.

In the case of seeded beams, where a heavy gas is accelerated by a light mass carrier gas during expansion, the mean energy of the heavy gas is given by:

$$\frac{1}{2} m_h \bar{V}_T^2 = \frac{m_h}{m_{\tilde{m}}} \int_o^T \bar{C}_{p_{\tilde{m}}} \, dT \tag{6}$$

where h and $\tilde{m}$ denote the heavy and mean gas. For the binary gas mixtures

$$\bar{m}_{\tilde{m}} = X_L m_L + X_h m_h \tag{7}$$

and,

$$\bar{C}_{p_{\tilde{m}}} = X_L C_{p_L} + X_h C_{p_h} \tag{8}$$

where X_L and X_h are the mole fractions of the light and heavy species, and m_L is the mass of the light gas.

For ideal expansion there will be no "velocity slip" between the light and heavy species. Then V_T represents the terminal velocity of both species in the beam. The effect of slip is to reduce the heavy species velocity from the ideal value. However, the velocity slip can be minimized by raising the source Reynolds number.

In the data reported, the energies and velocities are terminal values. That is, ideal expansion conditions were assumed. This is a reasonable assumption for low temperature cases (297°K). The actual values at high temperature (1400°K) may be off by about 5% at the most from the ideal values. Thus, the reported beam fluxes and flow rates at various points along the beam axis are also for ideal expansion conditions and are also accurate to 5%.

The isentropic relations for a perfect gas give the gas properties as a function of Mach number and stagnation conditions.

$$\frac{N}{N_o} = \left(1 + \frac{\gamma - 1}{2} M^2\right)^{-1/(\gamma-1)} \tag{9}$$

$$\frac{a}{a_o} = \left(\frac{T_o}{T}\right)^{-1/2} = \left(1 + \frac{\gamma - 1}{2} M^2\right)^{-1/2} \tag{10}$$

$$\bar{v} = Ma$$

where $\bar{v}$ is the flow velocity, a is speed of sound at temperature, T, and the subscript o indicates source conditions.

The flow rate through the nozzle at the throat may be calculated by noting that at the throat M = 1 and hence the total flow can be written:

$$F_N \text{ (molecules/sec)} = A_t \bar{v} N_t = A_t a_o N_o \left(\frac{\gamma + 1}{2}\right)^{-(\gamma+1)/2(\gamma-1)} \tag{11}$$

and the flux is equal to:

$$f_N \text{ (molecules/cm}^2\text{-sec)} = F_N/A_t \tag{12}$$

where A_t is the throat area in square centimeters. Finally the number density can be written:

$$N_t \text{ (molecules/cm}^3\text{)} = N_o \left(\frac{\gamma + 1}{2}\right)^{-1/\gamma-1} \tag{13}$$

where:

$$N_o = \frac{P_o}{kT_o} \tag{14}$$

For flow conditions along the centerline beyond throat for (L/D) > 4 where D is the diameter of nozzle and L is the downstream length from the throat:

$$M \cong \left[\left(\frac{\gamma + 1}{48}\right)\left(\frac{\gamma - 1}{2}\right)^{\gamma/(\gamma-1)}\right]^{-(\gamma-1)/2} \left(\frac{L}{D}\right)^{\gamma-1} \tag{15}$$

Since M is known the number density N (molecules/cm^3) at any L can be calculated using equation (9). Then the mean flux f_N (molecules/cm^2-sec) is equal to $N\bar{v}$. where $\bar{v} = v_T$ (the terminal velocity). Table VI shows the working equations used to calculate flow properties for H_e and H_2 seeded beams.

TABLE VI

BEAM PROPERTIES FOR $\gamma = 5/3$ AND $\gamma = 7/5$

	$\gamma = 5/3$	$\gamma = 7/5$
Nozzle flow	$F_N = 0.562\, A_T\, a_o\, N_o$	$F_N = 0.578\, A_T\, a_o\, N_o$
Mach number (for L/D > 4)	$M = (3.2)\left(\frac{L}{D}\right)^{2/3}$	$M = (3.64)\left(\frac{L}{D}\right)^{2/5}$
Centerline flux (for L/D > 4)	$f_N = 1.95\, \frac{F_N}{L^2}$	$f_N = \frac{1.78\, F_N}{L^2}$

The actual velocity and final translational temperature of the species after expansion must be determined from a time-of-flight analysis. Mean velocities and temperatures of the gases at the end of expansion are obtained from velocity distribution measurements using a time-of-flight technique. In this technique, the beam is chopped into small pulses. These pulses spread according to their velocity distribution as they travel over their flight distance. The detector measures the signal as a function of the arrival time. Thus, The signal versus time gives a direct measure of the velocity distribution function, the only difference being that it is now in a transformed time space.

The experimental setup is shown in Fig. 2. The setup is similar to one used by Anderson and Fenn and Gallagher, and has been described in detail elsewhere.[17] In the present setup, the flight path was 68 cm. The detector was a simple ionization gauge in the Bayerd-Alpert configuration. The shutter is an aluminum disk 7.5 in. in diameter and 1/16 in. thick with 4 slots each 0.079 in. wide on the periphery at 90° intervals. The shutter is mounted on the shaft of a synchronous motor energized by a variable frequency power supply.

The signal from the detector goes immediately to a cathode follower which employs a FET. The whole circuit is mounted very close to the detector in the vacuum system itself. The output of the FET is introduced to a low noise amplifier (PAR model CR 4A). After amplification, the signal is finally processed using the eductor. The details of the theory of time-of-flight velocity distributions are discussed by Anderson and Fenn.[18]

Examples of typical TOF experiments are illustrated by the eductor output traces shown in Fig. 3. The number density as a function of time of arrival is numerically analyzed using the approach of Subbarao and Miller.[19] The output of eductor traces such as that shown in Fig. 3 were reduced to velocity distribution data using a computer program based on this analysis.

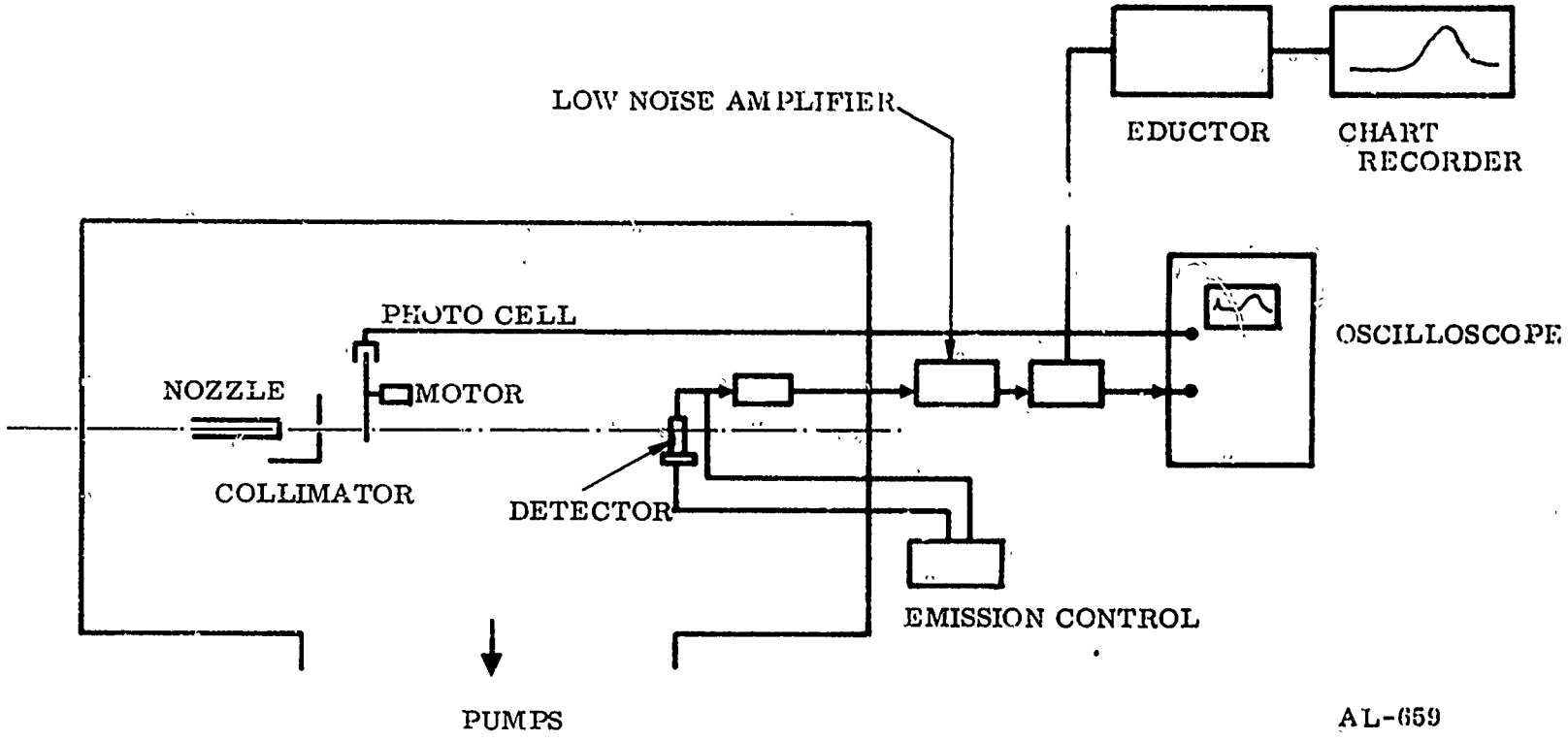

FIGURE 2 SKETCH OF SET UP FOR NOZZLE BEAM TIME-OF-FLIGHT VELOCITY CALIBRATIONS

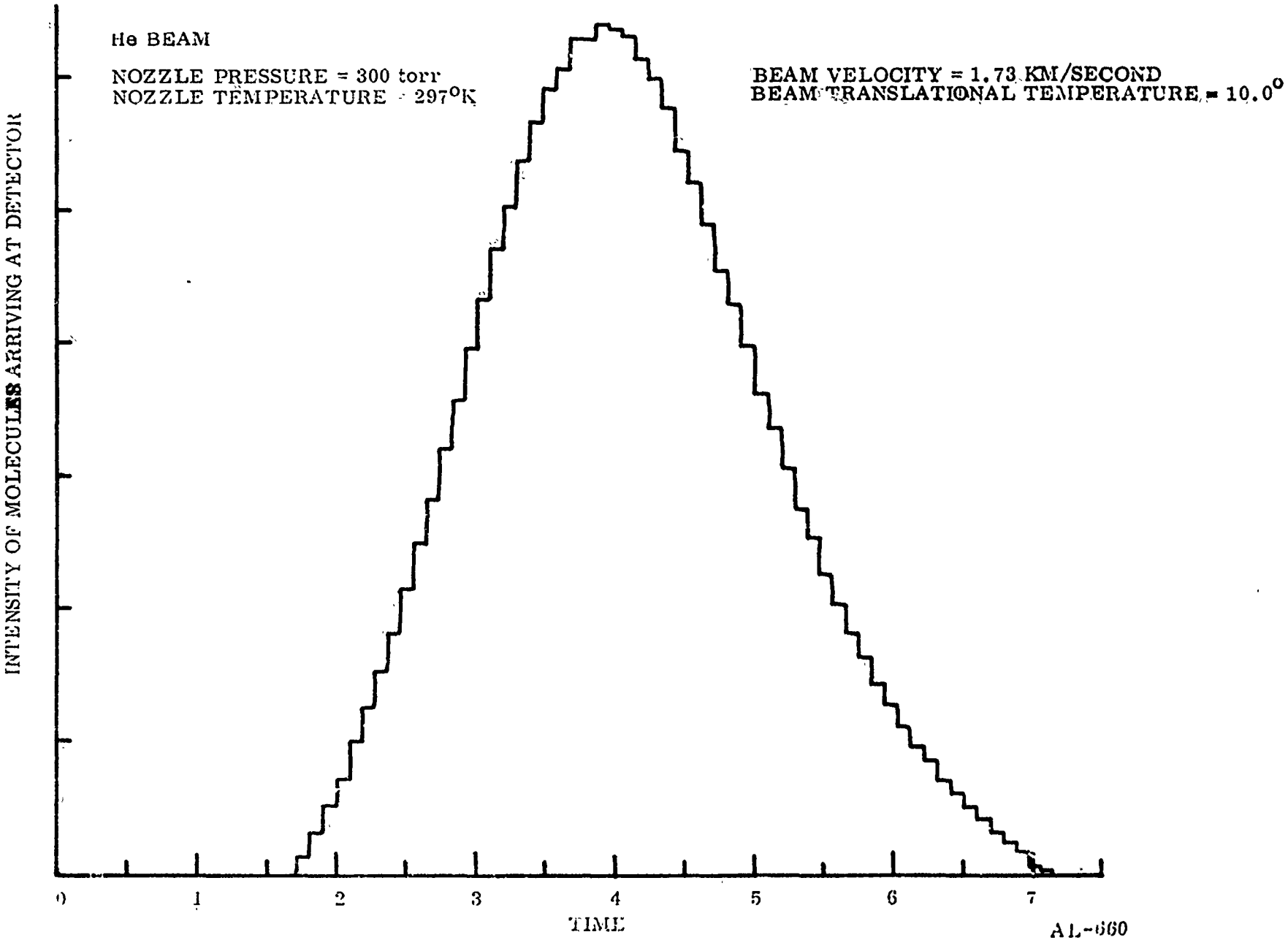

FIGURE 3A HELIUM NOZZLE BEAM TIME-OF-FLIGHT SPECTRUM

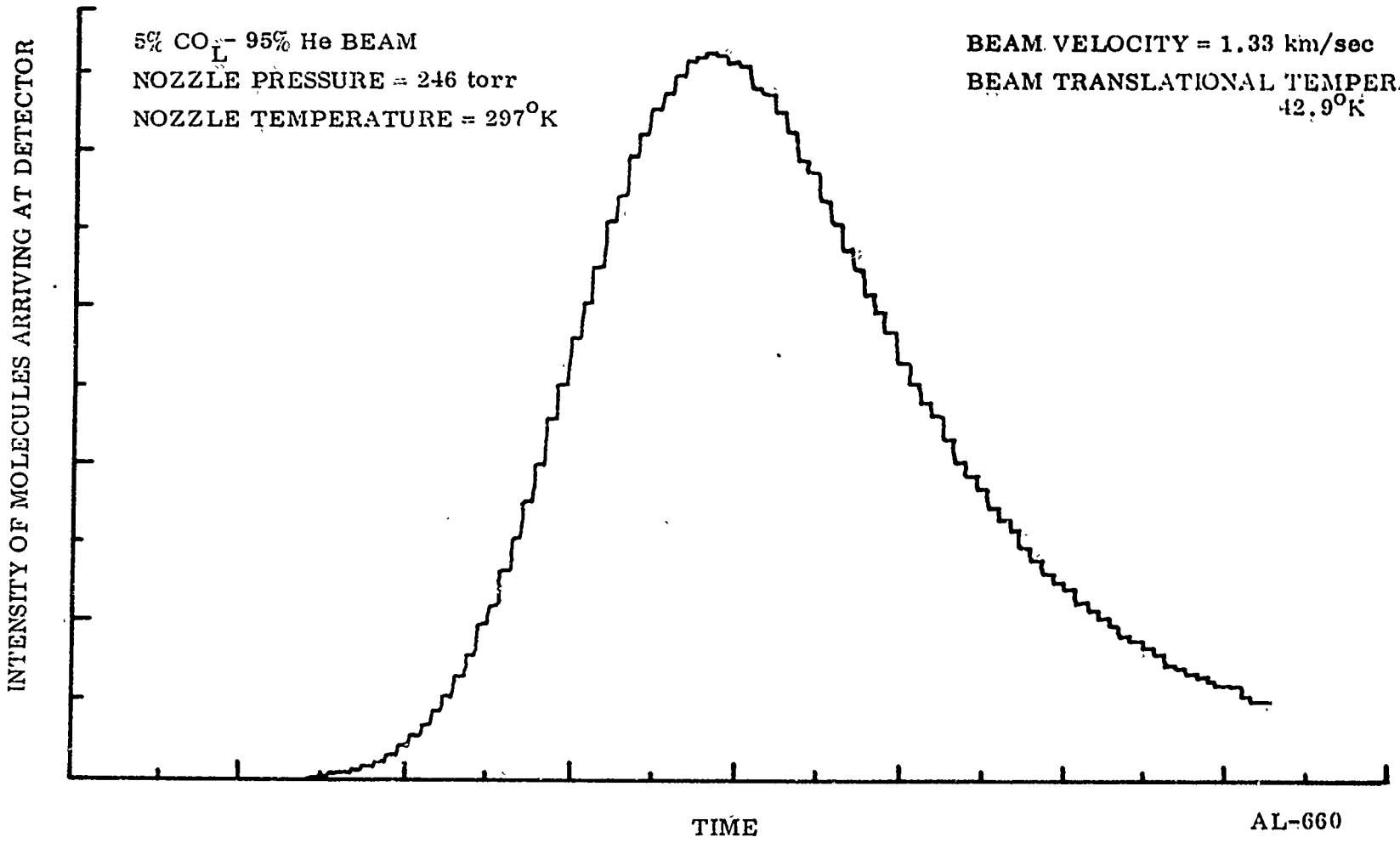

FIGURE 3B 5% CO_2, 95% He NOZZLE BEAM TIME-OF-FLIGHT SPECTRUM

3.2 Arc Discharge Atomic Oxygen Beam Source

A dozen or more recent experimental studies have indicated that open valance shell atomic species such as O, F, Cl, and Fe are much more effective in quenching excited molecular vibrational modes than closed shell molecules containing the same atoms. If the quenched vibrational energy is converted into translational energy for the atomic quenchant (V-T exchange) rather than molecular rotational energy, the reverse process of T-V exchange would be expected to be more effective for atomic species than molecular species at comparable collision energies. To be more specific, the observation that atomic oxygen is more efficient than either O_2 or N_2 in quenching CO_2 vibrations[13,14] may mean that O atoms are more effective than O_2 or N_2 in collisionally activating CO_2 vibrations. As shown in Table II, the Calspan experiment did indicate O atoms are more effective than N_2 molecules for the collisional excitation of the H_2O 2.7μ modes.

The desire to use atomic oxygen as a collision partner for studies of the collisional excitation of H_2O and CO_2 led to the design and fabrication of a dc arc discharge system to produce high intensity beams of molecular oxygen seeded in noble gas flows. The design and testing of this arc is the subject of this subsection.

The arc nozzle head is a modified Model 91 Plasma Torch manufactured by TAFA/Jonarc. Major modifications of the standard commerical unit include: 1) the addition of an O_2 inlet line and circular plenum designed to inject molecular oxygen into the normal noble gas discharge flow; 2) the addition of an exhaust gas exit flow chamber drained by two exhaust flow lines; 3) the addition of a water cooled nozzle insert in place of the normal torch outlet; and, 4) the installation of O-ring seals at all material joints to provide a vacuum tight unit.

An illustration of the nozzle end of the arc head is shown in Fig. 4. A noble gas flow at approximately 1 atmosphere is maintained past the arc cathode (not shown) and through the cylindrical anode. A dc discharge between the cathode and anode heats the noble gas to temperatures between 2000 and 5000^{o}K depending on the discharge current. A small amount of O_2 is injected into this hot flow and thermally dissociated. The noble gas-O atom mixture is directed at a nozzle insert which contains a pinhole on the order

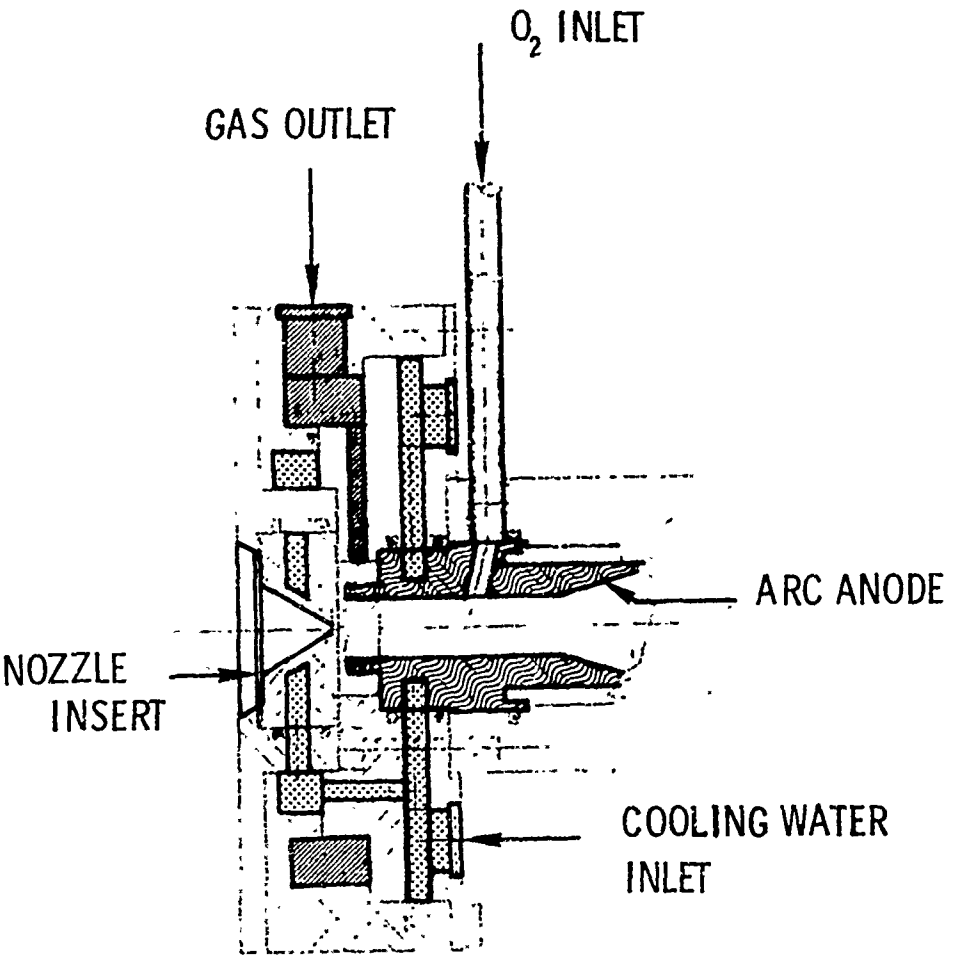

FIGURE 4 ANODE, OXYGEN INLET AND NOZZLE DESIGN FOR THE ATOMIC OXYGEN ARC BEAM SOURCE

of 0.005 in. in diameter. A small portion of the flow expands supersonically through the pinhole into the diverging cone shown in Fig. 4 and then on into the collision chamber. The remaining flow is pumped out through an anular exhaust chamber into exhaust lines which are designed to convey the exhaust gas out of the collision chamber. Figure 4 illustrates the nozzle, O_2 inlet and anode design for the arc source. The cathode end of the arc was the same as the standard TAFA Model 91 Plasma Torch.

Typical noble gas flows through the arc are 1 to 2 liter/sec. This produces flows that are approximately 10% atomic oxygen.

The arc powered by two TAFA Model 30-1A 14 kw dc power supplies and ignited by a 1000 amp high frequency starter. Gas flows are handled with a TAFA Model 47-50 Control Console equipped with suitable rotameters and needle valves for flow monitoring and control.

After the installation of power transformers, arc igniter, and gas handling system to operate the TAFA Model 91 Plasma Torch were completed at Yale, the plasma torch was operated successfully with both Ar and He. The plasma arc was stable over several hours of operation at the rated output. However, it is found that the copper nozzle inserts were eroded very rapidly by the hot plasma containing atomic oxygen. Within 20 min of operation, the nozzle throat diameter increased from 0.003 in. to 0.01 in. This increase in diameter caused an increase in mass flow into the vacuum chamber resulting in background pressures up to 10^{-4} torr. This high background pressure prevented the operation of a mass spectrometer and, hence, the analysis of the beam. Therefore, no measurements could be done to obtain the degree of dissociation of O_2 and the final flux of O atoms.

The erosion problem may well be overcome by replacing the copper nozzles with nozzle inserts of other materials. In further work nozzle inserts of tungsten, rhenium and various refractory oxides would be fabricated and tested for their ability to withstand the oxygenated plasma flow.

3.3 Vacuum System Description

The vacuum collision chamber is a steel cylinder 32 in. in diameter and 50 in. long. A NRC H-32-SP diffusion pump maintained the pressure in the chamber around 5×10^{-7} torr with no gas flow. Background pressure down to 3×10^{-7} torr can be reached using a liquid nitrogen trap. A 412 H Stokes mechanical pump with a pumping speed of 300 ft^3/min provided the backing for the diffusion at the foreline. Nominal pumping speed of the diffusion pump is 30,000 liter/sec at beam chamber pressures of 2×10^{-6} to 2×10^{-4} torr. A freon cooled optical baffle at the inlet to the diffusion pump approximately halves the available pumping capacity.

A NRC No. 518P ionization gauge and No. 710 gauge control are used to monitor background pressure in the vacuum chamber. With both beams on the background pressure, the chamber is typically about 2×10^{-5} torr.

3.4 Infrared Detection System and Data Collection Electronics

The infrared detector used in this study was a 2 mm diameter photovoltaic InSb high impedance chip with a nearly constant photon to electron quantum conversion efficiency of approximately 0.32 in the range from 1.5 to 5μ . The detectibility of radiation at 6μ was specified to be at least 3 orders of magnitude below that for 5μ radiation. The detector was mounted in an end viewing stainless steel liquid nitrogen dewar which allowed the chip to be cooled to 77°K and operate with a 60° field-of-view. The detector chip and dewar were supplied by the Santa Barbara Research Center.

In order to avoid noise limitations from background infrared radiation, the detector was integrated into the liquid nitrogen cooled optical train shown in Fig. 5. The detector dewar was operated without a window and evacuated by the collision chamber pumps through the viewing port which would normally be sealed by an optical window. The front face of the dewar served as a vacuum seal when it compressed on O-ring at the bottom of the detector housing shown in Fig. 5.

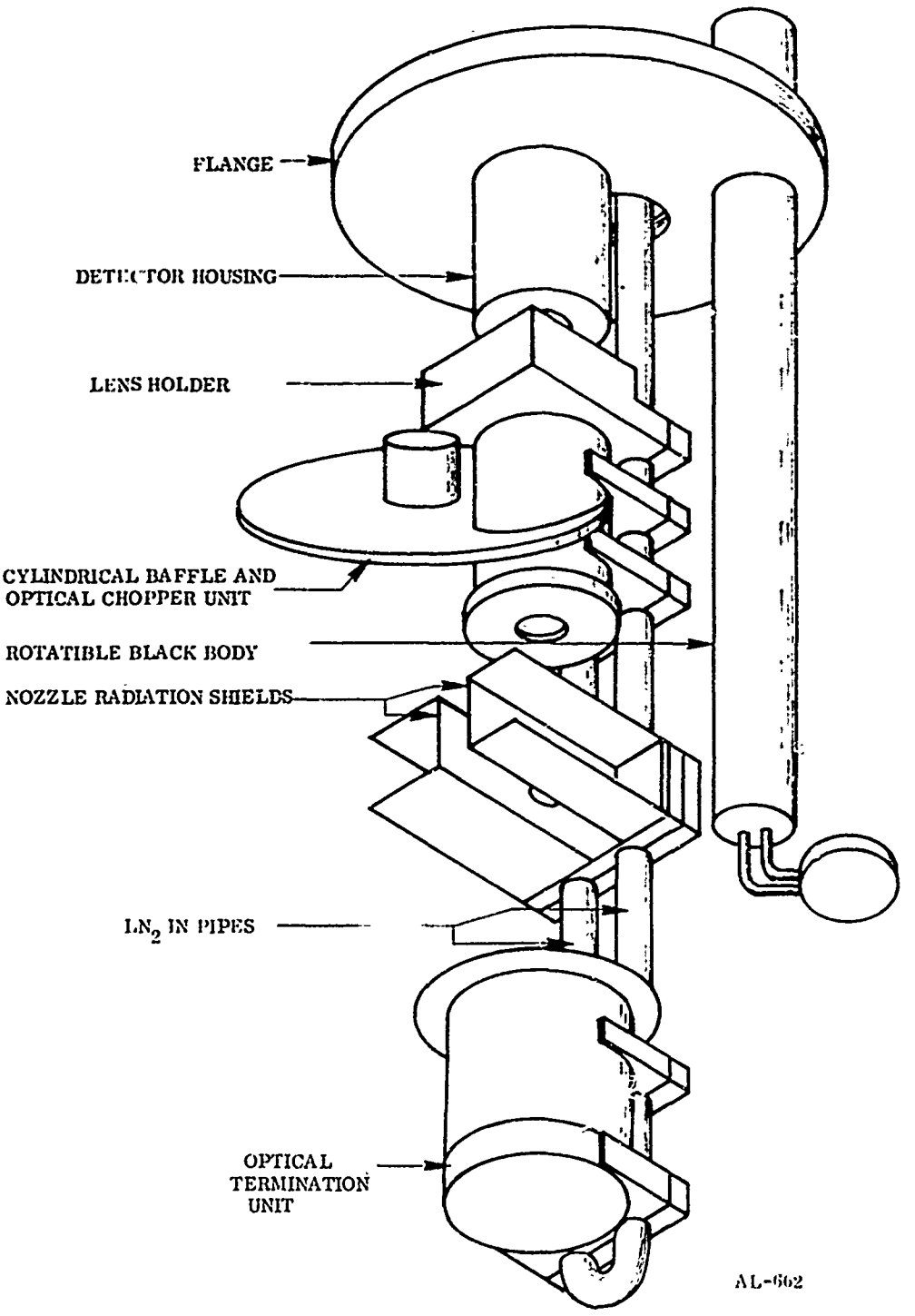

FIGURE 5 SKETCH OF INFRARED OPTICAL TRAIN

All of the optical components below the detector housing shown in Fig. 5 were mechanically clamped to a hollow 5/8 in. o.d. stainless steel U-tube which was suspended from a 1.5 liter liquid nitrogen dewar on top of the optical flange. Conduction from the 77°K, liquid nitrogen filled tube allowed all of the optical train components to be cooled to below 125°K, as determined by in vacuo thermocouple readings. Each of these components, with the obvious exception of lens and filters were fabricated from aluminum to take advantage of that material's high thermal conductivity. The clamps which mated the optical system components to the rigid U-tube were designed to allow alignment adjustments in three dimensions.

The optical train components in descending order below the detector housing were a lens holder, a cylindrical baffle unit which included a rotating, radiatively cooled optical chopper enclosed in a cooled housing, powered by a 40 Hz synchronous electric motor and an infrared filter holder, a set of radiation shields for the supersonic nozzles which supported an additional IR baffle, and an optical train termination unit which consisted of a baffled 3 in. diameter cylinder closed at the bottom. The infrared emissivity of all interior IR baffled surfaces, the chopper surface and the radiation shield surfaces were increased to near unity by coating with Black Velvet optical spray paint supplied by the 3M Company.

The lens holder unit supported and cooled two 2-in. diameter, 2-in. focal length meniscus silicon lenses which were supplied and antireflective coated by Optical Industries, Incorporated. These lenses were placed back-to-back, separated by a thin aluminum ring and supported 1.1 in. below the detector chip. This arrangement focused an interaction area 1.1 cm in diameter and 6 in. below the lens system center onto the detector chip. This interaction area was the centerpoint for the molecular beam interaction region in all subsequent experiments. The transmissivity of the lens unit was measured to be 0.21 for both 2.7 and 4.3μ radiation during system calibration tests. The lens assembly fixed the acceptance solid angle of the optical train at 0.084 sr for light emitted from the beam interaction region.

The infrared optical path between the interaction area and the lens holder was filled by a 2 in. cylindrical baffle unit. Separate 1-in. infrared filters with 0.13μ bandpasses at 2.7 and 4.3μ, respectively, supplied by Infrared Industries, Incorporated, were mounted directly above this aperature when needed for calibration measurements. A set of two ring baffles could also be mounted inside the 2 in. baffle unit between the filter holder and the lens holder. Radiation passing through this baffle unit could be chopped by a radiation cooled, low temperature two bladed chopper whose housing was supported by the baffle unit. The chopper was powered by a 40 Hz synchronous motor and the chopping frequency was monitored by a passive magnetic pick-up unit supplied by Electrosales, Incorporated.

Below the cylindrical baffle unit at the level of the beam interaction region were two infrared radiation baffles designed to minimize the radiation into the optical train emitted from the hot nozzle beam sources. Beam exit holes through these baffles were masked with razor blade slits in an effort to minimize scattered radiation while maintaining desirable flow conditions.

A space below the nozzle baffles was left open to allow the placement of a blackbody unit which could be rotated in and out of the optical path as illustrated in Fig. 5. This blackbody unit could be varied in temperature between 77 and 320^{o}K by flowing controlled amounts of liquid N_2 or heated N_2 gas through access tubes at the top of the optical system flange. The temperature of the blackbody was measured with a calibrated chromel-constantan brazed to the unit. The blackbody, itself, was a stainless steel cylinder whose upper flat surface was viewed by the detector. The emissivity of this surface was improved by treatment with 3M Black Velvet optical paint. The blackbody and the optical train chopper were used only in detector calibration procedures and both were turned out of the optical path during the molecular beam experiments.

Finally, below the blackbody space, the optical system terminated in a baffled 3 in. diameter cylindrical unit closed at the bottom, whose inside surfaces were black.

The current responsivity of the detector and its associated optical train was measured for 2.7 and 4.3μ radiation before the optical flange was installed in the molecular beam scattering chamber. A vacuum test stand designed to accommodate the optical flange was used for this calibration procedure. Radiation from the rotatable blackbody

at a known temperature was passed through the 2.7 or 4.3μ IR filters with 90% band-passes of 0.13μ. This filtered radiation was alternately passed and stopped with the cooled radiation chopper and the difference in detector current response was measured with a Kiethly Model 171 digital voltmeter operated in its ammeter mode. The measured detector current responsivities were 0.953 amp/w of incident 4.3μ radiation and 0.600 amp/w of incident 2.7μ radiation. These responsivities were measured for blackbody, in-band radiation fluxes from $5\text{x}10^{-11}$ to $6\text{x}10^{-9}$ w. When combined with the 0.21 silicon lens transmissivity measurement, the optical system current responsivity becomes 0.202 amp/w for 2.7μ radiation and 0.126 amp/w of 4.3μ radiation emitted into the system's field-of-view.

In normal operation, the output of the detector was fed into a Santa Barbara Research two-stage amplifier designated Model 9906. The 9906 unit was designed to have a preamp output of:

$$V_{pa}\ (\text{volts}) = I_{det.} \times 2.57 \times 10^{8}, \tag{16}$$

where I_{det} is the InSb detector output in amps. The preamplifier stage was followed by a post-amp stage with a gain of 100, so the total design output signal, V_{out}, could be written in terms of the detector output current, I_{det}, as:

$$V_{out}\ (\text{volts}) = I_{det} \times 2.57 \times 10^{10} \tag{17}$$

The amplifier unit was designed to accept radiation modulated at a frequency between 4 and 900 Hz. Unmodulated radiation was not amplified; however, a dc infrared flux above 20 nw was sufficient to overload the preamp circuit. This placed a severe requirement on liquid N_2 cooled IR baffling which had to shield the detector from all room temperature surfaces.

The 9906 amplifier unit did produce an output voltage as calculated by Eq. (16) when connected to a current source with infinite output resistance. However, when the 9906 amplifier was connected to the InSb detector and calibrated with known IR radiation fluxes corresponding to known detector current outputs, a somewhat lower amplication of:

$$V_{out}\ (\text{volts}) = I_{det} \times 2.75 \times 10^{9} \tag{18}$$

was obtained. This loss of amplification is believed to be the result of a mismatch between the 9906 preamplifier feedback resistor and the effective InSb chip resistance. Its effect is to lower the effective responsivity by a factor of 9.

Two forms of noise limit the infrared detector and optics system as it is presently employed. The first and most serious of these is the scattering of chopped infrared radiation originating from the collision partner nozzle. The problem becomes more severe for higher collision velocities since a chopped nozzle source must then be operated at higher temperatures, producing more infrared radiation. Extensive cooled IR baffling and improved nozzle radiation shields did reduce the magnitude of scattered light by about a factor of 50, to about 1 nw from a 1400°K nozzle source. However, the problem remains the limiting noise source for most experiments, since collision induced radiation must be detected as an added signal to this "in phase" noise source.

A second serious source of noise is a random pulse or shot noise associated with the detector even the absence of illuminating radiation. According to Santa Barbara Research personnel, this noise appears to be associated with electrical breakdown in the detector chip due to contamination of the InSb chip by diffusion pump oil, and may be improved by detector bias voltage adjustments.

A waveform eductor (PAR Model TD H-9) was used to process the output signal from the preamplifier. The eductor is a form of multichannel signal averager. In essence, it consecutively samples the input signal over 100 equal intervals each time the repetitive waveform occurs, separately integrates the samples to suppress noise and stores each averaged sample in its memory. As the average of any random noise is zero, the contents of the memory asymptotically approaches the point-by-point value

of the repetitive waveform itself. A photo-cell signal (from G.E. Photon coupled interrupter module No. H13A1) at chopper 2 establishes time zero and is used to trigger the eductor. The output of the eductor was recorded on a strip chart x-y recorder (Mosley Model 7101A).

A lock-in amplifier (PAR Model 122) with phase-sensitive detection was also available for processing the signal. However, the maximum allowable input signal to this model amplifier is limited to 50 mV, and since the signals handled were often more than 50 mV, its usage was not always possible.

4. DATA ANALYSIS TECHNIQUES

4.1 Detector Response Functions

The photon flux falling on the InSb detector, F_{det}, is proportional to the number of vibrationally excited molecules, N_{ex}, in the detector's field-of-view:

$$F_{det}\left(\frac{\text{photons}}{\text{sec}}\right) = \frac{N_{ex}}{\tau_{rad}} \quad \frac{\Omega}{4\pi} \quad T, \tag{19}$$

where Ω is the solid acceptance angle in steradians for the lens-detector system, and T is the transmission factor for the optical components. As noted in the preceding section, Ω can be calculated as 0.084 sr and for operation without filters, T is the lens transmission factor which was measured as 0.21 for both 2.7 and 4.3μ radiation.

$$P_{det}\,(\text{watts}) = \frac{N_{ex}\; h\nu_o}{\tau_{rad}} \quad \frac{\Omega}{4\pi} \quad T. \tag{20}$$

If no filters are used and radiation from more than one excited state in the 1.5 to 4.4μ detector's sensitivity range is contributing to the detector flux, then Eq. (20) is generalized to:

$$P_{det}(\text{watts}) = \frac{\Omega}{4\pi} \quad T \sum_i \quad \frac{N_{ex\ i}\,(h\,\nu_o)_i}{\tau_{rad\ i}} \tag{21}$$

Since the electron to photon quantum efficiency is constant in the 1.5 to 5μ range, the detector's current responsivity, R_λ, which relates photon power on the detector to detector current output is proportional to photon wavelength. As noted in the preceding section, R_λ was measured for 4.3 and 2.7μ as 0.953 and 0.600 amp/w, respectively.

R_λ can be linearly extrapolated from these values for other wavelengths in the 1.5 to 5.0μ range. Multiplication of Eq. (21) by the appropriate R_λ values yields the detector current output, I_{det} :

$$I_{det}(\text{amps}) = \frac{\Omega}{4\pi} \quad T \sum_i \frac{R_{\lambda\, i} N_{ex\, i} \quad (h\nu_o)_i}{\tau_{rad\, i}} \tag{22}$$

As noted in the preceding Section, I_{det} is related to the voltage output of the detector-amplifier system by a simple multiplicative factor as shown in Eq. (18) to yield:

$$V_{out}\ (\text{volts}) = 2.75 \times 10^9 \quad \frac{\Omega}{4\pi} \quad T \sum_i \quad \frac{R_{\lambda_i} N_{ex\, i} (h\nu_o)_i}{\tau_{rad_i}} \tag{23}$$

Evaluating Eq. (23) for the no filter case where using the values of T and Ω noted above yields:

$$V_{out}\ (\text{volts}) = 3.86 \times 10^6 \sum_i \quad \frac{R_{\lambda\, i} N_{ex\, i} \quad (h\nu_o)_i}{\tau_{rad\ i}} \tag{24}$$

4.2 Dynamic Calibration Technique

In order to expedite calibration measurements a procedure designed to use the self-emission of a beam of hot CO_2 or H_2O as a calibration radiation source was devised and tested. At the highest nozzle source temperatures of 1400 to 1500°K used in this study the equilibrium population of the H_2O (ν_1 and ν_3) and CO_2 (ν_3) modes are nearly 2% and 8%, respectively. While it is possible that a portion of these vibrationally excited species will be quenched during the supersonic expansion process, if this quenching is not too severe, the self-emission of a chopped hot H_2O or CO_2 beam is an ideal calibration source since its spatial and spectral characteristics are nearly identical to the expected cross beam emissions. Quenching of vibrationally excited CO_2 or H_2O could arise from two sources: collisional quenching during the first stages of the supersonic expansion or radiative quenching during the flow time between the nozzle and the detector field of view. Radiative quenching effects can be shown to be negligible since the flow time is on the order of 10^{-5} sec for both hot H_2O and CO_2 beams (a flow distance of ~4 cm divided by an average velocity of 4×10^5 cm/sec). The radiative lifetimes of CO_2 and H_2O ν_3 modes from Table I are 2.4×10^{-3} and 17×10^{-3} sec respectively, so that the ratios of the flow times to the characteristic

radiative lifetimes are 0.004 for CO_2 and 0.0006 respectively showing that radiative quenching is not important. Collisional quenching should also be unimportant, since as indicated in Table IV, even the most efficient quenching partners require between 30 and 300 collisions on an average to quench CO_2 (ν_3) or H_2O (ν_3). Thus, it is doubtful that sufficient collisions are available to produce significant quenching in the rapidly expanding nozzle flow. It should be noted that this H_2O or CO_2 self-emission was not detected in cross beam experiments because the hot exhaust gas beam was not modulated and the self-emission signal was part of the dc background. If no H_2O or CO_2 vibration quenching during the nozzle expansion process is assumed, the expected photon flux on the detector from a modulated H_2O or CO_2 beam can be calculated from Eq. (24) where N_{ex} for each contributing vibrational mode is expresses as:

$$N_{ex}(\text{chopped exhaust beam}) = n_1 \, V \, e^{-h\nu_c/kT}, \qquad (25)$$

where n_i is the density of exhaust type molecules in the detector's field-of-view, V is the volume of the field-of-view and T is the nozzle temperature. The field-of-view volume was calculated from lens and detector parameters to be 1.05 cm^3, while n_1 can be calculated from Eq. (9) and the terminal beam velocity. Measurement conditions and resulting detector system voltages are shown in Table VII.

TABLE VII

DYNAMIC CALIBRATION CONDITIONS

Gas Mixture	Nozzle Pressure (T, °K)	Nozzle Temperature (T, °K)	Exhaust Gas Beam Density (n_1, cm^3)	Observed Output Voltage (v_{out}, volts)
0.05 CO_2/0.95 H_2	776	1325	1.84×10^{11}	0.590 ± 0.010
0.05 H_2O/0.95 H_2	660	1325	1.36×10^{11}	0.032 ± 0.010

These calibration measurements were made without filters, so it is important to decide which of the vibrationally active modes listed in Table I could have contributed to the observed signal. Ignoring possible differences in quenching rates, the population of each state in the beam is proportional to $e^{h\nu_0/kT}$ and the production of photons from these excited states is inversely proportional to the radiative lifetimes listed in Table I. Using these parameters, it was possible to estimate relative contributions to the observed signal. The result for CO_2 was that the ν_3 mode accounts for well over 99% of the CO_2 signal, while the ν_3 mode of H_2O accounts for over 80% of the H_2O signal,

with the ν_1 mode and the 011 combination band emission each accounting for approximately 10%. All other modes of CO_2 and H_2O were calculated to be able to produce less than 1% to the observed emissions.

The characteristics of the pertinent CO_2 and H_2O states needed to calculate N_{ex} for each mode are shown in Table VIII.

TABLE VIII

MODE CHARACTERISTICS FOR CALIBRATION N_{ex} CALCULATIONS

Molecule	Mode	$h\nu_o/kT$	$h\nu_o$ (joules)
CO_2	ν_3	0.0781	4.67×10^{-20}
H_2O	ν_3	0.0170	7.46×10^{-20}
	ν_1	0.0190	7.25×10^{-20}
	001	0.0031	10.57×10^{-20}

Substituting the parameters from Tables VII and VIII into Eq. (25) the following values of N_{ex} are calculated for the pertinent CO_2 and H_2O modes:

CO_2 Calibration beam: $N_{ex}(\nu_3) = 1.51 \times 10^{10}$

H_2O Calibration beam: $N_{ex}(\nu_3) = 2.43 \times 10^{9}$

$N_{ex}(\nu_1) = 2.71 \times 10^{9}$

$N_{ex}(001) = 4.43 \times 10^{8}$ (26)

These values of N_{ex} were substituted into Eq. (24) along with appropriate values of τ_{rad} from Table I, $h\nu_o$ from Table VIII and R_λ as noted in the text to yield the following calculated values of output voltages for the CO_2 and H_2O calibration beams:

CO_2 Calibration beam:
$$\frac{v_{out}\ (obs.)}{v_{out}\ (calc.)} = 0.55 \pm 0.01$$

H_2O Calibration beam:
$$\frac{v_{out}\ (obs.)}{v_{out}\ (calc.)} = 1.13 \pm 0.35 \qquad (27)$$

where the stated uncertainties are those listed for the v_{out} measurement.

The ratios listed above show close agreement between the dynamic beam calibration and the expected signal value based on blackbody calibration parameters. Black body calibrations were performed by inserting the rotatable blackbody into the detector field of view with either the 2.7 or 4.3 filter in place and measuring the detector output current as a function of blackbody temperature. This technique allowed calculation of the detector current responsivities and optical throughput factors presented in Subsection 3.4 because the infrared power on the detector could be calculated from the blackbody Planck formula, the bandpass of the filters and the solid angle of the detector-lens system. The close agreement indicates that there is very little CO_2 or H_2O vibrational quenching in the nozzle expansions, and that the beam self-emissions can be used as an in situ calibration source in place of the cooled blackbody arrangement. The advantages of this calibration scheme are outlined in the following subsection.

4.3 Collision Signal Analysis

The expected collision-induced signal from the intersecting flow experiment can also be calculated from Eq. (24) with the appropriate expression for N_{ex}. Letting n_1, n_2 again represent the number density of collision partners, σ_i represents the total collision cross section for the excitation of the i^{th} vibrational mode, v_r represents the relative precollision velocity of the beams of exhaust species and collision partners, V_c represents the collision volume of the two intersecting beams, $\bar{v}$ represents the average post-collision velocity of the excited exhaust species and r represent the radius of the cylindrical detector field-of-view (0.503 cm); N_{ex} for each excited vibration mode can then by written as:

$$N_{ex\ i}(\text{intersecting beam}) = [n_1\ n_2\ \sigma\ v_r\ V_c]\ \frac{r}{\bar{v}} \qquad (28)$$

This derivation of N_{ex} ignores collisions between the light seed gas (usually H_2) and the exhaust species because for most experimental collision velocities these collisions will be below the energy threshold for vibrational activation. In the cases where such collisions are not below threshold, their effect can be experimentally subtracted by comparing emissions from runs that are identical except for the presence or absence of the heavy collision partner in the second beam.

The term in square brackets in Eq. (28) expresses the rate of creation of excited state molecules in the field-of-view, while the additional term expresses the average time these excited molecules spend in view, since they must travel an average distance r, at an average velocity $\bar{v}$ to leave the detector's field-of-view. Unlike the beam self-emission calibration, where, except for the negligibly small fraction of excited states which radiatively decay while in the field-of-view, the flux of excited molecules in and out of the field-of-view is identical, both the rate of excited state creation and their flux out of the field-of-view has to be considered in deriving Eq. (28). However, it is still true that the depletion of N_{ex} due to radiative decay was negligibly small.

The nozzle beams used in this experiment are reasonably well defined in spatial extent and the interaction volume seen by the InSb detector was designed to coincide with the intersection volume of the beams used in this study. The assumption that the beam intersection volume and the interaction volume seen by the detector are identical is made in the following calculations. This assumption breaks down most severely when the beam intersection angle is near 180°, but due to the diverging beam flow, it does not introduce unacceptable errors even in this case. This is due to the fact that beam flux per unit area in the scattering region decreases as approximately L^{-2}; where, as in Subsection 3.1, L is the center line distance from the nozzle. In these experiments the distance from the nozzle to the detector field of view was 4 cm. Thus, in the region 1 cm beyond the field-of-view the beam density will decrease to $(4/5)^2$ or 0.64 of the density in the field-of-view region. The beam density will further decrease to $(4/6)^2$ or 0.44 in the next cm. Collisions more than 2 cm from the nominal beam intersection area were not allowed because the beam was dispersed by the nozzles radiation shields. Furthermore, many of the molecules undergoing inelastic collisions in the regions outside the detector field-of-view will be scattered out of the beam and never enter the field of view. The maximum number of additional collisions resulting from the 180° geometry would be

2 x (0.64 + 0.44) or a factor of 2.2, however, as noted above most of the products of these collisions did not enter the detector's field of view, and therefore, did not interfere in the measurement.

Thus, the expected detector signal can be written as:

$$v_{out}(\text{intersecting beams}) = 3.86 \times 10^{6} \; V_c \, n_1 \, n_2 \; {}_r r \sum_i \frac{\sigma_i (h\nu_{o\,i}) R_{\lambda_i}}{\bar{v}_i \; \tau_{rad\;i}} \qquad (29)$$

where the subscripts i refer to quantities associated with the i^{th} vibrational mode. The experimental signal calculated with Eq. (29) can be compared with that calculated for the beam self-emission calibration which is found by substituting Eq. (25) into Eq. (24).

$$v_{out}\,(\text{beam self-emission}) = 3.86 \times 10^{6} \; n_1 \; V \sum_i \frac{e^{-(h\nu_o)_i/kT}}{\tau_{rad\;i}} \; (h\nu_o)_i \; R_\lambda \qquad (30)$$

Dividing Eq. (30) into Eq. (29) yields:

$$\frac{v_{out}(\text{beam self-emission})}{v_{out}(\text{intersecting beams})} = \frac{n_1(\text{bse})}{n_1\,(\text{ib})} \; \frac{1}{n_2 \, v_r \, r} \sum_i \frac{\bar{v}_i}{\sigma_i} \; e^{-(h\nu_o)_i/kT} \qquad (31)$$

since as previously noted V is assumed to be equal to V_c. The exhaust species beam densities are not assumed to be equal unless the exhaust gas nozzle conditions are the same for both calibration and experimental runs. The quantities n_2, v_r and $\bar{v}_i$ and σ_i are related only to the intersecting beam experiment, while T refers to the calibration run nozzle temperatures. The summation over various vibrational modes can be removed for the cases of H_2O and CO_2 by noting that if σ_i is not a strong function of vibrational mode, the radiation from CO_2 for both calibration and experimental runs will be >99% from the ν_3 mode because of its short radiative lifetime, while the greater than 80% of the radiation from H_2O will be due to the ν_3 mode for the same reason.

Thus, even without 2.7 or 4.3μ filters, the experiments performed in this study are quite specific to the ν_3 stretch modes of CO_2 and H_2O. The cross sections for exciting these modes can be expressed by inverting Eq. (31) to yield:

$$\sigma(\nu_3) \simeq \frac{v_{out}(\text{ib})}{v_{out}(\text{bse})} \; \frac{n_1\,(\text{bse})}{n_1\,(\text{ib})} \; \frac{\bar{v}}{n_2 \, r \, V_r} \; e^{-h\nu_o/kT} \; , \qquad (32)$$

The remaining obstacle to the use of Eq. (32) for experimental data analysis is the unknown exhaust species average post-collision velocity, $\bar{v}$. In order to evaluate $\bar{v}$, a kinematic analysis was performed for the intersecting beams. Such an analysis is relatively simple, in a formal sense, if performed in center of mass coordinates. For brevity's sake, the details of this analysis are not presented here, however, any result depends on the assumed form of the angular dependence of the differential cross section for vibrational excitation in center of mass coordinates. Since this angular dependence is unknown, it was assumed to be constant which leads to the following simple expression for $\bar{v}$:

$$\bar{v} = c/2 \tag{33}$$

where c is the center of mass velocity. For the maximum relative velocity case of the beam intersection angle at 180^{o}, this leads to an expression for $\bar{v}$ of:

$$\bar{v} = \left| \frac{m_1 v_1 - m_2 v_2}{2 (m_1 + m_2)} \right| \tag{34}$$

where m_1 and m_2 are the masses of the exhaust species and its collision partner, respectively, and v_1 and v_2 are the magnitudes of their associated beam velocities. Kinematic analyses for nonconstant center of mass differential cross sections indicate that the use of Eq. (34) for $\bar{v}$ will introduce, at most, a factor of three error in the determination of vibrational activation cross sections.

The combination of Eqs. (32) and (34) are the basic formulations used to reduce the experimental data presented in the following section.

5. EXPERIMENTAL RESULTS

A series of experiments using 5% N_2 / 95% H_2 seeded beams colliding at 180° with 5% CO_2 / 95% H_2 and 5% H_2O / 95% H_2 beams were performed and compared to the H_2O and CO_2 self-emission calibrations described in the previous section. No signals were observed which could be ascribed to collision induced emissions. The limit to the change in signal which would be detectable under the high noise conditions encountered was set at 0.005 V. The main contribution to this high background was chopped, scattered radiation from the hot nozzle sources as described in Section 3.

Upper limits to the cross section for activation of the CO_2 and H_2O ν_3 vibrational mode by N_2 were calculated for a number of relative velocities by substituting experimentally determined parameters into Eq. (32). The results of these determinations are summarized in Table IX. Center of mass collision energies and the ratios of collision energies to ν_3 activation threshold energies are also displayed.

TABLE IX

SUMMARY OF EXPERIMENTAL RESULTS

Exhaust Species	Collision Partner	Relative Collision Velocity (cm/sec)	Center of Mass Collision Energy (eV)	Ratio of Collision Energy to ν_3 Threshold Energy	Upper Limit to ν_3 Collision Cross Section (cm^2)
CO_2	N_2	5.86×10^5	3.04	10.4	1.1×10^{-15}
CO_2	N_2	7.83×10^5	5.43	18.7	3.6×10^{-15}
H_2O	N_2	4.09×10^5	0.96	2.1	2.5×10^{-15}
H_2O	N_2	6.62×10^5	2.50	5.4	2.5×10^{-14}
H_2O	N_2	6.76×10^5	4.38	9.4	2.7×10^{-14}

6. DISCUSSIONS AND RECOMMENDATIONS

6.1 Comparison of Results to Total Scattering Cross Sections

The upper limits to collision induced T-V excitation of the CO_2 and H_2O ν_3 vibrational modes can be compared to previously determined total scattering cross sections. The total scattering cross section for the CO_2 - N_2 system has been measured as 4.04×10^{-14} cm^2 at relatively low collision energies.[20] The total scattering cross section for the H_2O - N_2 system has not been determined, however, two measurements for the H_2O - H_2O[21,22] system and one for the H_2O - NH_3[21] are available. Since the H_2O - H_2O total scattering cross section shows little evidence of dipole-dipole interactions[22] it can be assumed that the N_2 - H_2O cross section is of similar magnitude, and an average of the values of Kydd[21] and Snow, et.al.[22] are used for the N_2 - H_2O cross section in Table X. Table X also shows the ratios of the smallest measured upper limits for ν_3 activation to the previously measured total scattering cross sections. These ratios represent an upper limit to the fraction of collisions which result in ν_3 T-V activation.

TABLE X

COMPARISON OF ν_3 EXCITATION CROSS SECTION LIMITS TO TOTAL SCATTERING CROSS SECTIONS

Section	V_r (cm/sec)	ν_3 Excitation Cross Section (σ_E) (cm^2)	Total Scattering Cross Section (σ_T) (cm^2)	σ_E/σ_T
CO_2/N_2	5.86×10^5	1.1×10^{-15}	4.04×10^{-14}	0.027
H_2O/N_2	4.09×10^5	2.5×10^{-15}	4.35×10^{-14}	0.057

The limits listed in Table X show that less than 3% of all N_2 - CO_2 collisions which are 10.4 times more energetic than the ν_3 vibrational threshold energy activate the CO_2 ν_3 mode, while less than 6% of all N_2 - H_2O collision cross sections with 2.1 times the ν_3 threshold energy available, result in excitation of the ν_3 mode.

6.2 Comments on the Experimental Technique

The upper bounds on the collisional excitation cross sections for the CO_2 and H_2O ν_3 modes found in this study are compatible with the cross sections previously measured by Dunn, et.al.[7] However, it is clear that these bounds are several orders of magnitude larger than the actual ν_3 T-V excitation cross sections. The crossed beam technique used in this study did provide reasonable fluxes of exhaust species and collision partners at relative velocities of 2 to 8 km/sec. The infrared detection system was shown to be sensitive to CO_2 and H_2O ν_3 radiation, and the self-emission of a hot CO_2 or H_2O beam was demonstrated to be a convenient in situ IR calibration source.

The limiting problem with the detection system used in this study was the interfering chopped radiation signal scattered into the detector field-of-view from the hot nozzle source. Extra nozzle radiation shielding and IR baffles were used to reduce this noise problem by about a factor of 50 during the experiment reported here. Redesign of the nozzle radiation shields and the adoption of a pulsed supersonic nozzle system such as that used by Hagena[23] should enable this noise source to be reduced by at least four orders of magnitude. This reduction in the chief noise source would enable the measurement of cross sections at least 10^{-4} smaller than the upper bounds measured in this study if no additional unexpected noise sources are encountered. Intrinsic detector noise produced by dc blackbody emissions in the optical train and scattering system are calculated to be well below 10^{-4} times the curred ac blackbody emission noise.

Further studies would also take care to avoid the detector chip contamination with diffusion pump oil which took place during optical equipment design experiments. Improved detector handling procedures would help reduce the high shot noise levels encountered with the current detector. In addition, because of detector problems encountered in the present study, Santa Barbara Research personnel have devised improved detector chip mounts for high sensitivity, low background applications.[24] Future studies would benefit from these detector design improvements.

6.3 Recommendations for Future Work

Redesign of the hot nozzle radiation shielding and the adoption of a pulsed rather than chopped nozzle source would improve the present experimental system to the point where H_2O and CO_2 ν_3 excitation cross sections on the order of 10^{-18} to 10^{-19} cm^2 are measureable. The system would then be capable of yielding definitive T-V excitation cross sections for these important rocket exhaust species.

In addition, further nozzle insert design work on the arc heated O atom nozzle source described in Subsection 3.2 should also allow the measurement of collisional excitation cross sections using O atoms for collision partners.

It is recommended that support for the redesign and upgrading of these nozzle and detector system components be provided while the experimental equipment and personnel assembled for the present study are still available to finish the needed measurement program.

7. REFERENCES

1. S.S. Penner, Quantitative Molecular Spectroscopy and Gas Emissivities, p. 19-21, Addison-Wesley, Reading, Mass. (1959).

2. G. Herzberg, Infrared and Raman Spectra of Polyatomic Molecules, p. 274 and 281, Van Nostrand-Reinhold, N.Y., (1945).

3. J. E. Lowder, J. Quant. Spec. Rad. Trans., 11, 153 (1971).

4. D. M. Gates, R. F. Calfee, D.W. Hansen, and W.S. Benedict, Line Parameters and Computed Spectra for Water Vapor Bands at 2.7 , N.B.S. Monograph, 71, U.S. Govt. Print. Office, Washington, D.C., (1964)

5. D.F. Eggers, Jr., and B. L. Crawford, Jr., J. Chem. Phys. 19, 1554 (1951).

6. R.F. Calfee and W.S. Benedict, Carbon Dioxide Spectral Line Positions and Intensities Calculated for the 2.05 and 2.7 Regions, N.B.S. Technical Note, 332, U.S. Govt. Printing Office, Washington, D.C., (1966).

7. M. G. Dunn, G.T. Skinner and C.E. Treanor, Infrared Radiation from H_2O, CO_2 or NH_3 Collisionally Excited by N_2, O, or Ar, Rept. No. TE-5073-A-4, Calspan Corporation, (1973).

8. R. Marriot, Proc. Phys. Soc. 84, 877 (1964); 86, 1041 (1965), 88, 83 and 617 (1966).

9. E. R. Fisher, A Review of Vibrational Cross Sections Involving H_2O, CO_2, H_2, CO and He, Wayne State University, Rept. No. AFCRL-72-0539, (1972)

10. J. N. Bass, J. Chem. Phys. 60, 2913 (1974).

11. K. S. Tait, C.E. Kolb, and H.R. Baum, J. Chem. Phys. 59, 3128 (1973).

12. R.E. Center, and R. V. Kung, Private communication (1973).

13. R.E. Center, J. Chem. Phys., 59, 3523 (1973).

14. J. H. W. Crump and J. D. Lambert, Chem. Phys. Let. 22, 146 (1973).

15. D. F. Heller and C.B. Moore, J. Chem. Phys. 52, 1005 (1970).

16. M. I. Buchwald and S. H. Bauer, J. Phys. Chem. 76, 3108 (1972).

17. R. J. Gallagher, Ph.D. Thesis, Yale University, (1972).

18. J. B. Anderson, and J. B. Fenn, Physics of Fluids, 8, 780 (1965).

19. R. B. Subbarao, and D. R. Miller, The Journal of Chemical Physics, 58, 5247 (1973).

20. H. E. Berek, J.T. Dowell, L.H. Frae, G.F. Hagner and W.R. Snow, Bull. Am. Phys. Soc. 18, 141 (1973).

21. P. H. Kydd, J. Chem. Phys. 37, 931 (1962).

22. W. R. Snow, J.T. Dowell, J. G. Chevrenak and H.E. Berek, J. Chem. Phys. 58, 2517 (1973).

23. K. Bier and O. Hagena, Rarefied Gas Dynamics Vol. II, 106, (1966, J. H. DeLeeuu, editor, Academic Press, New York.

24. D. Skvarna, Santa Barbara Research Center, Private communication (1974).